Mass Measurement of ^{56}Sc Reveals a Small $A = 56$ Odd-Even Mass Staggering, Implying a Cooler Accreted Neutron Star Crust

Z. Meisel,[1,2,3,*] S. George,[1,3,4] S. Ahn,[1,3] D. Bazin,[1] B. A. Brown,[1,2] J. Browne,[1,2,3] J. F. Carpino,[5] H. Chung,[5] A. L. Cole,[6] R. H. Cyburt,[1,3] A. Estradé,[7] M. Famiano,[5] A. Gade,[1,2] C. Langer,[1,3] M. Matoš,[8,†] W. Mittig,[1,2] F. Montes,[1,3] D. J. Morrissey,[1,9] J. Pereira,[1,3] H. Schatz,[1,2,3] J. Schatz,[1] M. Scott,[1,2] D. Shapira,[10] K. Smith,[3,11,‡] J. Stevens,[1,2,3] W. Tan,[11] O. Tarasov,[1] S. Towers,[5] K. Wimmer,[1,§] J. R. Winkelbauer,[1,2] J. Yurkon,[1] and R. G. T. Zegers[1,2,3]

[1]National Superconducting Cyclotron Laboratory, Michigan State University, East Lansing, Michigan 48824, USA
[2]Department of Physics and Astronomy, Michigan State University, East Lansing, Michigan 48824, USA
[3]Joint Institute for Nuclear Astrophysics, Michigan State University, East Lansing, Michigan 48824, USA
[4]Max-Planck-Institut für Kernphysik, 69117 Heidelberg, Germany
[5]Department of Physics, Western Michigan University, Kalamazoo, Michigan 49008, USA
[6]Physics Department, Kalamazoo College, Kalamazoo, Michigan 49006, USA
[7]School of Physics and Astronomy, The University of Edinburgh, EH8 9YL Edinburgh, United Kingdom
[8]Department of Physics and Astronomy, Louisiana State University, Baton Rouge, Louisiana 70803, USA
[9]Department of Chemistry, Michigan State University, East Lansing, Michigan 48824, USA
[10]Oak Ridge National Laboratory, Oak Ridge, Tennessee 37831, USA
[11]Department of Physics, University of Notre Dame, Notre Dame, Indiana 46556, USA

(Received 31 May 2015; published 16 October 2015)

We present the mass excesses of $^{52-57}$Sc, obtained from recent time-of-flight nuclear mass measurements at the National Superconducting Cyclotron Laboratory at Michigan State University. The masses of ^{56}Sc and ^{57}Sc were determined for the first time with atomic mass excesses of $-24.85(59)(^{+0}_{-54})$ MeV and $-21.0(1.3)$ MeV, respectively, where the asymmetric uncertainty for ^{56}Sc was included due to possible contamination from a long-lived isomer. The ^{56}Sc mass indicates a small odd-even mass staggering in the $A = 56$ mass chain towards the neutron drip line, significantly deviating from trends predicted by the global FRDM mass model and favoring trends predicted by the UNEDF0 and UNEDF1 density functional calculations. Together with new shell-model calculations of the electron-capture strength function of ^{56}Sc, our results strongly reduce uncertainties in model calculations of the heating and cooling at the ^{56}Ti electron-capture layer in the outer crust of accreting neutron stars. We find that, in contrast to previous studies, neither strong neutrino cooling nor strong heating occurs in this layer. We conclude that Urca cooling in the outer crusts of accreting neutron stars that exhibit superbursts or high temperature steady-state burning, which are predicted to be rich in $A \approx 56$ nuclei, is considerably weaker than predicted. Urca cooling must instead be dominated by electron capture on the small amounts of adjacent odd-A nuclei contained in the superburst and high temperature steady-state burning ashes. This may explain the absence of strong crust Urca cooling inferred from the observed cooling light curve of the transiently accreting x-ray source MAXI J0556-332.

DOI: 10.1103/PhysRevLett.115.162501 PACS numbers: 21.10.Dr, 26.60.Gj

The thermal structure of the crust of neutron stars that accreted matter from a nearby companion star directly relates to a number of astronomical observables, including the ignition of frequently observed type-I x-ray bursts [1–5], x-ray superbursts [6–11], the observed cooling of transiently accreting neutron stars while accretion is turned off [12–19], and, potentially, gravitational wave emission [20,21].

The crust of accreting neutron stars strongly differs in composition and thermal structure from isolated neutron stars. The composition is set by the ashes of hydrogen and helium burning on the surface via the rapid proton capture process (rp process), the αp process, and helium fusion reactions [22,23]. With increasing depth, the rising electron Fermi energy E_{Fermi} induces electron-capture reactions at specific locations where E_{Fermi} matches the energy thresholds for electron capture. The result is a layered composition of more and more neutron rich nuclei that preserves the mass numbers A of the thermonuclear ashes at the surface [24–28]. At still greater depths, beyond neutron-drip density, release and capture of neutrons, as well as pycnonuclear fusion reactions, lead to further changes in composition. While matter is accreted, these reactions operate continuously throughout the crust, maintaining its steady-state composition profile. The associated nuclear energy release heats the crust to higher temperatures than the neutron-star core. Alternatively, in some cases, depending on the nuclear physics [29], an electron capture–β-decay Urca cycle [30] can occur in the thin layer around a compositional boundary that leads to rapid neutrino cooling instead of heating.

Of particular importance are the reaction sequences along the $A = 56$ mass number chain in the outer crust. $A = 56$ nuclei are predicted to make up a significant portion of the outer crust in many neutron stars because they are copiously produced for a range of hydrogen and helium burning conditions at the neutron star surface, including steady-state burning at high accretion rates or high temperatures [22] as is the case for the quasipersistent transient MAXI J0556-332 [31,32], type-I x-ray bursts, and superbursts [22,33–36].

As in all even-A mass chains, the odd-even staggering of electron-capture energy thresholds, a consequence of the nuclear pairing energy, leads to significant crust heating in the $A = 56$ reaction chain. At a depth where E_{Fermi} just exceeds the threshold for electron capture $Q_{\mathrm{EC}}(Z, A) = \mathrm{ME}(Z, A) - \mathrm{ME}(Z - 1, A)$ on an even-even nucleus, the odd-odd nucleus formed by electron capture is immediately destroyed by a second electron-capture reaction with a lower threshold (see Fig. 1). For this second step, E_{Fermi} exceeds the threshold, and the energy difference is split between the escaping neutrino and heat deposition into the crust. The energy release therefore corresponds directly to the magnitude of the odd-even staggering of the electron-capture thresholds. For the $A = 56$ chain of electron captures, thresholds are only known experimentally to ^{56}Ti. Predictions for the odd-even staggering $\Delta Q_{\mathrm{EC}} = Q_{\mathrm{EC}}(Z - 1, A) - Q_{\mathrm{EC}}(Z, A)$ beyond ^{56}Ti vary dramatically (see Fig. 4). While density-functional calculations predict a rather constant evolution of ΔQ_{EC}, the finite-range droplet mass model (FRDM) [38] predicts a significant increase, and the Hartree-Fock-Bogoliubov (HFB) mass model, labeled HFB-21 [40], predicts a dramatic drop. It is worth noting that even though ΔQ_{EC} is a double difference of masses, predictions vary by almost 6 MeV, an order of magnitude larger than the sometimes quoted global mass-model error [38] and the related rms deviations of global mass model predictions from known masses.

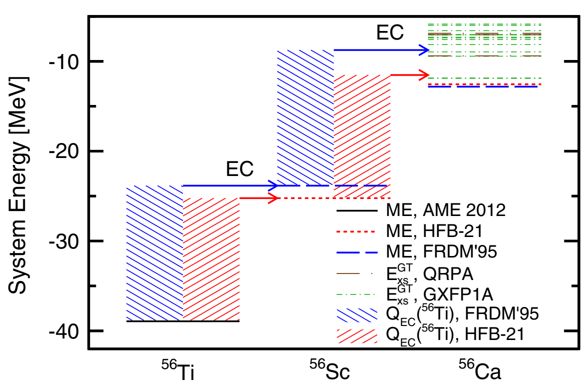

FIG. 1 (color online). Energy levels for the $A = 56$ mass chain at a depth where $E_{\mathrm{Fermi}} \approx |Q_{\mathrm{EC}}(^{56}\mathrm{Ti})|$, where atomic mass excesses ME are shown for the 2012 Atomic Mass Evaluation (AME) [37] (solid black line) if known experimentally and for theoretical mass models otherwise. The larger odd-even mass staggering for the FRDM mass model [38] (long-dashed blue line) allows the second of the sequential electron captures (EC) to proceed through Gamow-Teller (GT) transitions, shown here for shell-model calculations using the GXPF1A Hamiltonian [39] (dot-dashed green line) and for the QRPA calculations used in [29] (dot-dashed brown line), to higher-lying excited states $E_{\mathrm{xs}}^{\mathrm{GT}}$ in ^{56}Ca than for the HFB-21 mass model [40] (short-dashed red line).

Electron-capture thresholds are modified when the first available transition proceeds through an excited state of the daughter nucleus, typically the lowest-lying state with nonnegligible transition strength [27], rather than through the ground state. In most cases, this does not change the general picture of a two-step electron capture sequence in even mass chains. However, with the relatively small ΔQ_{EC} between ^{56}Ti and ^{56}Sc predicted by the HFB-21 mass model (2.65 MeV), and the relatively high excitation energy of the lowest-lying strength of the $^{56}\mathrm{Sc} \to {}^{56}\mathrm{Ca}$ transition (3.4 MeV) predicted by their global quasiparticle random-phase approximation (QRPA) model, Schatz *et al.* [29] point out an unusual situation where the electron capture on odd-odd ^{56}Sc is blocked at the depth where ^{56}Sc is produced by electron capture on ^{56}Ti, preventing a two-step electron capture sequence (see Fig. 1). As a consequence, they [29] find that ^{56}Sc β decay leads to a strong Urca cycle between $^{56}\mathrm{Ti} + e^- \to {}^{56}\mathrm{Sc} + \nu_e$ and $^{56}\mathrm{Sc} \to {}^{56}\mathrm{Ti} + e^- + \bar{\nu}_e$, resulting in rapid neutrino cooling in neutron star crusts with $A = 56$ material. This effect disappears when employing the large ΔQ_{EC} predicted by the FRDM mass model [29].

To address the large uncertainties in the predicted ΔQ_{EC} for $A = 56$, we performed a measurement of the ^{56}Sc mass. In addition, we carried out new shell-model calculations of the ^{56}Sc electron-capture strength function which, in connection with the new mass results, lead to much improved predictions of heating and cooling of $A = 56$ nuclei in neutron star crusts.

The masses of $^{52–57}$Sc were obtained with the time-of-flight (TOF) method at the National Superconducting Cyclotron Laboratory [41–43]. The experimental setup and analysis are described in more detail in [41,43,44] and are only summarized briefly here. A broad range of ~150 neutron-rich isotopes from silicon to zinc were produced by fragmentation of a 140 MeV/u ^{82}Se beam on a beryllium target, transmitted through the A1900 fragment separator [45], and then sent to the focal plane of the S800 spectrograph [46]. The fully stripped ions were identified event by event using their time of flight (TOF) measured with fast-timing scintillators along a 60.6 m flight path L_{path} and their energy loss in an ionization chamber. The magnetic rigidity $B\rho$, being the ratio of momentum p over charge q, of each ion was determined relative to the tune of the beam line through a position measurement using

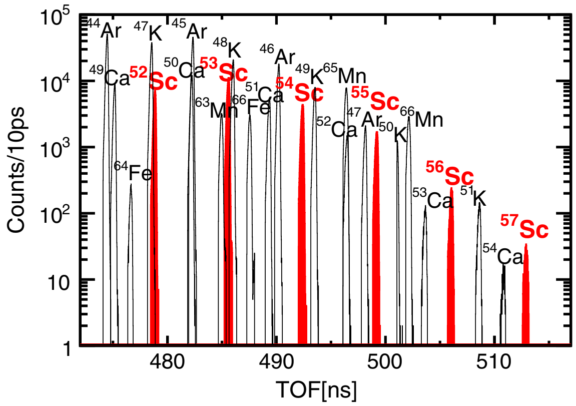

FIG. 2 (color online). Rigidity-corrected time-of-flight distributions for reference nuclei (unfilled histograms) used to calibrate the m_{rest}/q(TOF) relationship to obtain masses from the TOFs of the $A = 52–57$ isotopes of scandium (red-filled histograms).

a microchannel plate detector [47] at the dispersive focus at the S800 target position [44].

The ion rest mass is related to TOF and $B\rho$ through $m_{rest} = (\mathrm{TOF}/L_{path})[q(B\rho)/\gamma]$, where γ is the Lorentz factor. Because neither L_{path} nor $B\rho$ are absolutely known with sufficient accuracy, the (m_{rest}/q)(TOF) relationship is determined empirically using reference nuclei with well-known masses [43].

The TOF distributions for reference nuclei and $^{52-57}$Sc are shown in Fig. 2. Twenty reference nuclei with masses known to better than 100 keV and no known isomeric states longer lived than 100 ns [37,48,49] were fitted with a seven-parameter calibration function of first and second order in TOF, first order in TOF $*$ Z, and containing first, second, and fourth order Z terms. The calibration function represents a minimal set of terms that minimized the overall fit residual to literature masses and resulted in no detectable systematic biases [41], as seen in Fig. 3. Additional energy loss in the A1900 wedge degrader, which was not present in [41,42], required the addition of the TOF $*$ Z fit term. A systematic uncertainty of 9.0 keV$/q$ was included as described in [41] to normalize the χ^2 per degree of freedom of the mass fit to one. Two additional uncertainties related to the extrapolation were added to the final mass uncertainties, one to reflect the uncertainties in the TOFs of reference nuclei, which leads to an uncertainty in the fit coefficients of the m/q(TOF) relation, and one to reflect the uncertainty inherent in choosing a particular calibration function over another which has a comparable goodness of fit. The latter was determined by investigating the robustness of the results to adding additional terms to the calibration function. The total mass uncertainty is a sum in quadrature of statistical, systematic, and two extrapolation uncertainties. The relative contribution of the extrapolation uncertainties becomes larger as the distance in m/q and Z from reference nuclei increases.

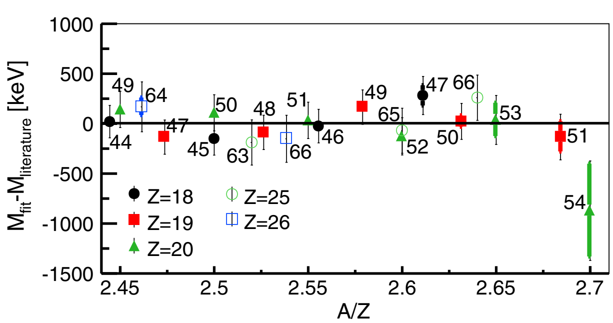

FIG. 3 (color online). Residuals of the fit to the m/q-TOF relationship of calibration nuclei ($^{44-47}$Ar, $^{47-51}$K, $^{49-54}$Ca, ^{63,65,66}Mn, and ^{64,66}Fe) as a function of the mass number to nuclear charge ratio A/Z. Thick colored error bars show statistical uncertainties. Thin black error bars show the sum in quadrature of the statistical uncertainty and the systematic uncertainty, 9 keV$/q$ (here $q \equiv Z$), included for reference nuclei as described in [41].

The atomic mass excesses for scandium isotopes determined in this experiment are compared to experimental and theoretical literature values in Table I. We note that the measured values reported for ^{56}Sc and ^{57}Sc are a significant advancement over the extrapolated values reported in the 2012 AME [37], as the AME extrapolation assumes a locally smooth mass surface [37] and frequently fails in regions demonstrating changes in nuclear structure (e.g., ^{53}Ca and ^{54}Ca [48] as compared to the 2003 AME [52]), such as the region covered by this work in which the $N = 32$ and $N = 34$ neutron subshell closures are weakly constrained [53]. The mass uncertainties presented here correspond to a measurement precision of $\delta m/m \approx 1 \times 10^{-5}$. The primary contribution to the overall measurement uncertainty comes from the uncertainty inherent to the mass-fit extrapolation owing to the limited number of reference nuclei with similar Z and A/Z. An additional uncertainty for ME(^{56}Sc) originates from the presence of a β-decaying isomer of unknown excitation energy [53,54] that may be populated in the fragmentation reaction producing ^{56}Sc. ^{56}Sc has a β-decaying low-spin (1^+) state and a β-decaying high-spin (5^+ or 6^+) state, but it is not known which is the ground state and which is the isomeric state. Shell-model calculations with the GXPF1A Hamiltonian [39] predict an excitation energy of the isomer of 540 keV. The resolution of the ^{56}Sc TOF peak is 100 ps, corresponding to a mass resolution of 10 MeV, and can therefore not be used to constrain the relative population of the ground and isomeric states. Thus, the atomic mass excess obtained in this Letter represents a least-bound limit for the ^{56}Sc ground state and, guided by theory, we add an asymmetric uncertainty of $^{+0}_{-540}$ keV to our result to account for the unknown population ratio. The resulting atomic mass excess of ^{56}Sc determined in this Letter is $-24.85(59)(^{+0}_{-54})$ MeV. As seen in Table I, the atomic mass excess of ^{56}Sc presented here is consistent with the

TABLE I. Atomic mass excesses (in keV) of scandium isotopes measured in this experiment compared to results from previous direct mass measurements [Time-of-flight Isochronous Spectrometer (TOFI) [50], Experimental storage ring (ESR) [51], and National Superconducting Cyclotron Laboratory (NSCL) [42]], the adopted value in the 2012 Atomic Mass Evaluation (AME) [37] ("E" are extrapolations), and predictions from global mass models (FRDM [38] and HFB-21 [40]). The asymmetric uncertainty included for the ^{56}Sc mass excess is an additional systematic uncertainty from potential isomeric contamination.

Isotope	This experiment	TOFI	ESR	NSCL	AME 2012	FRDM	HFB-21
^{52}Sc	−40 300 (520)	−40 520 (220)	…	…	−40 170 (140)	−39 360	−40 110
^{53}Sc	−38 170 (570)	−38 600 (250)	−38 840 (110)	−38 110 (270)	−38 110 (270)	−36 840	−38 480
^{54}Sc	−33 750 (630)	−33 500 (500)	−34 520 (210)	−33 540 (360)	−33 600 (360)	−32 030	−33 980
^{55}Sc	−30 520 (580)	−28 500 (1000)	…	−30 240 (600)	−29 980 (460)	−29 170	−31 320
^{56}Sc	−24 850 (590)$(^{+0}_{-540})$	…	…	…	−24 731E (401E)	−23 840	−25 230
^{57}Sc	−21 000 (1300)	…	…	…	−20 707E (503E)	−20 440	−22 550

prediction from the HFB-21 [40] global mass model, but is more bound than the prediction from the FRDM [38] global mass model.

Our result for ME(^{56}Sc) can be used to calculate the odd-even staggering of Q_{EC} in the $A = 56$ mass chain. $Q_{EC}(^{56}\mathrm{Ti}) = -14.4(^{+1.3}_{-0.7})$ MeV is now determined exclusively from experimental data. For $Q_{EC}(^{56}\mathrm{Sc})$, we still need the theoretical mass prediction for ^{56}Ca. However, the large discrepancy for $Q_{EC}(^{56}\mathrm{Sc})$ between various mass models is exclusively due to the large discrepancies in the predictions for the ^{56}Sc mass, since predictions for the atomic mass excess of ^{56}Ca ME(^{56}Ca) agree within ≈300 keV [38,40]. We therefore can combine our new ^{56}Sc mass with the ^{56}Ca mass predicted by either the FRDM or HFB-21 mass models and find similar values of $-12.0(^{+0.6}_{-1.1})$ MeV and $-12.3(^{+0.6}_{-1.1})$ MeV, respectively. For the two choices of ^{56}Ca mass, this results in a Q_{EC} staggering of $\Delta Q_{EC}(^{56}\mathrm{Sc}) = Q_{EC}(^{56}\mathrm{Sc}) - Q_{EC}(^{56}\mathrm{Ti}) = 2.3(^{+1.3}_{-2.4})$ MeV and $2.1(^{+1.3}_{-2.4})$ MeV, respectively. Figure 4 shows the evolution of ΔQ_{EC} in the $A = 56$ mass chain for odd-Z nuclei as a function of Z, where we have included both of the aforementioned $\Delta Q_{EC}(^{56}\mathrm{Sc})$ in an attempt to capture the contribution of

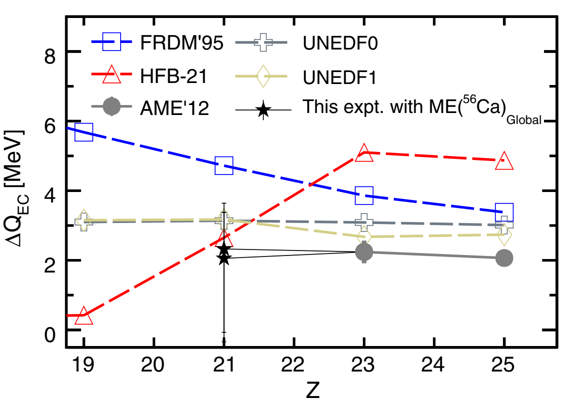

FIG. 4 (color online). $\Delta Q_{EC}(Z, A)$ for odd-odd $A = 56$ nuclei using ME(^{56}Sc) from this experiment and ME(^{56}Ca) from FRDM'95 or HFB-21 (black stars), compared to global mass models [38,40] and mass differences predicted from recent energy density functional calculations [55,56] (open shapes).

the theoretical mass uncertainty of ^{56}Ca. The new data rule out the rapid increase in ΔQ_{EC} approaching the neutron drip line predicted by FRDM, and rather favor the predictions of recent energy density-functional-based binding-energy calculations [55,56] of a fairly constant ΔQ_{EC} along $A = 56$.

The implications of $\Delta Q_{EC}(^{56}\mathrm{Sc})$ obtained here for the accreted neutron star crust were explored by inclusion of our result for ME(^{56}Sc) in calculations performed with the state-of-the-art crust composition evolution model presented in [27,29,42]. The model follows the compositional evolution of an accreted fluid element with increasing pressure $p = \dot{M}gt$, where the accretion rate $\dot{M} = 2.64 \times 10^4\ \mathrm{g\,cm^{-2}\,s^{-1}}$, surface gravity $g = 1.85 \times 10^{14}\ \mathrm{cm\,s^{-2}}$, and time t, at a constant temperature of $T = 0.5$ GK (from [27]) using a full reaction network that includes electron capture, β decay, neutron capture and their inverse, and fusion reactions. These conditions are in the range inferred for the present population of observed quasipersistent transient sources [19]. The ^{56}Ti electron-capture layer was found to be either Urca cooling with more than 7 MeV per accreted nucleon (HFB-21 mass model), or heating with 0.05 MeV per accreted nucleon (FRDM mass model) [29] (see Fig. 5, FRDM,HFB-21 column). The reason for this very large discrepancy is that in the FRDM mass model $\Delta Q_{EC}(^{56}\mathrm{Sc}) = 4.3$ MeV is larger than the excitation energy of the lowest-lying electron-capture transition in ^{56}Ca predicted by the QRPA model used in previous studies (3.4 MeV), while in the HFB-21 mass model it is lower (2.6 MeV), as was demonstrated in Fig. 1. With the HFB-21 masses electron capture on ^{56}Sc is therefore blocked initially and an effective Urca cycle involving ^{56}Ti and ^{56}Sc ensues. Our results for $\Delta Q_{EC}(^{56}\mathrm{Sc})$, when combined with the QRPA model, in principle are closer to the HFB-21 case (see Fig. 5, Expt + QRPA column).

However, heating and cooling at electron-capture transitions in neutron star crusts also depend sensitively on the electron-capture and β-decay strength functions. In particular, the small odd-even mass stagger for $A = 56$ nuclei found in this Letter can lead to strong Urca cooling

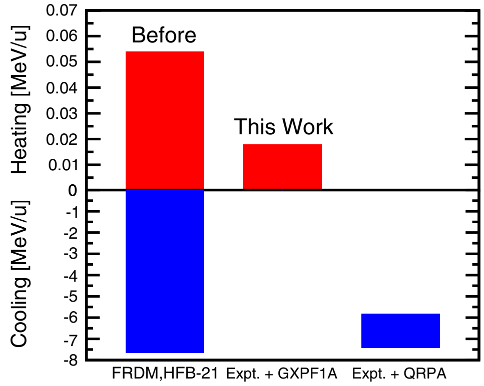

FIG. 5 (color online). Integrated energy per accreted nucleon released from (negative values) or deposited into (positive values) the neutron star crust at the ^{56}Ti → ^{56}Sc → ^{56}Ca compositional transition at a fiducial temperature of 0.5 GK and an accretion rate of 0.3 $\dot{M}_{\mathrm{Eddington}}$. The left column indicates the large uncertainty prior to our work, where either heating or strong cooling were possible depending on the choice of global mass model for predicting ME(^{56}Sc) (FRDM [38] or HFB-21 [40]) or on the choice of GT-transition strengths (shell-model using the GXPF1A Hamiltonian [39] or the QRPA [29]). The right and central columns show the narrow range of integrated heating or cooling possible when employing ME(^{56}Sc) reported here (within $\pm 1\sigma$ uncertainty) and GT transitions from QRPA or the more reliable shell-model calculations performed for this study that employ the GXPF1A Hamiltonian.

depending on the location and strength of electron capture and β-decay transitions. Previous studies employed predictions of a global QRPA model because of its availability for the entire range of nuclei of relevance for neutron star crusts. However, for the particular case of the electron capture on ^{56}Sc of interest here, more reliable shell-model calculations are possible [57]. We performed such calculations using the GXPF1A effective interaction [39] and, using our new masses, find no Urca cooling (see Fig. 5, Expt + GXPF1A column). This is because the shell model predicts a 1^+ ground state for ^{56}Sc and therefore a strong allowed electron-capture transition to the ground state of ^{56}Ca that removes nuclei quickly from the ^{56}Ti–^{56}Sc Urca cycle. Indeed, a 1^+ ground state for ^{56}Sc is consistent with experimental data, while the spin 3 prediction from the QRPA model is not.

When using the shell-model strength function, our new ^{56}Sc mass significantly reduces uncertainties in predictions of nuclear heating. In particular, it excludes the relatively strong heating predicted by the FRDM mass model, and limits heating to less than 0.02 MeV per accreted nucleon. Within mass uncertainties, no heating or even weak cooling (0.002 MeV$/u$) from prethreshold electron capture are possible. These results do not depend significantly on our crust model assumptions, as heating is given per accreted nucleon and is therefore independent of accretion rate, and heating is relatively insensitive to the crust temperature.

In principle, experimental data do not exclude the possibility that the 1^+ state in ^{56}Sc is the long-lived isomer and a 5^+ or 6^+ high spin state is the ground state [53,54]. In this case, selection rules would prevent a ground-state–to–ground-state electron-capture transition from ^{56}Sc to ^{56}Ca. However, even if the 1^+ state in ^{56}Sc is a low-lying, long-lived excited state instead of the ground state, it will likely be thermally excited at temperatures in excess of 0.3 GK where Urca cooling is relevant, again leading to rapid depletion of the ^{56}Ti–^{56}Sc Urca cycle via an electron-capture transition to the ^{56}Ca ground state. Additionally, for the case of a 5^+ ground state, the shell model predicts a strong electron-capture transition into a 1.25 MeV excited state in ^{56}Ca which could also be populated by electron capture given our reported odd-even mass stagger, thereby precluding Urca cooling as well. Our shell-model-based results are therefore robust.

In summary, we have addressed the very large uncertainties in the impact of the ^{56}Ti electron-capture layer on the thermal structure of accreting neutron star crusts reported in [29] through a measurement of the ^{56}Sc mass and shell-model calculations of the ^{56}Sc electron-capture strength. In contrast to previous studies, we find that neither strong cooling nor strong heating occurs in this layer. The thermal structure of accreting neutron stars with superbursts or high temperature steady-state burning, which produce large amounts of $A = 56$ material, therefore depends sensitively on the coproduction of smaller amounts of odd-A nuclei around $A = 56$ that will dominate Urca cooling in the outer crust. To quantify this effect it is now crucial to reliably predict the abundance of odd-A nuclei produced in the thermonuclear processes on the surface of accreting neutron stars.

Overall, we find that Urca cooling in $A = 56$-dominated accreted neutron star crusts is much weaker than previously predicted. This may explain the absence of strong Urca cooling recently inferred from the x-ray cooling light curve of the transiently accreting system MAXI J0556-332 [31,32], which is thought to host high temperature steady-state burning.

This project is funded by the NSF through Grants No. PHY-0822648, No. PHY-1102511, No. PHY-1404442, and No. PHY-1430152. S. G. acknowledges support from the DFG under Contracts No. GE2183/1-1 and No. GE2183/2-1. We thank Erik Olsen for providing nuclear binding energies from energy density functional calculations and E. F. Brown and A. T. Deibel for many useful discussions.

*zmeisel@nd.edu
Present address: Department of Physics, University of Notre Dame, Notre Dame, Indiana 46556, USA.

[†]Present address: Physics Division, International Atomic Energy Agency, 1400 Vienna, Austria.
[‡]Present address: Department of Physics and Astronomy, University of Tennessee, Knoxville, Tennessee 37996, USA.
[§]Present address: Department of Physics, University of Tokyo, Hongo 7-3-1, Bunkyo-ku, 113-0033 Tokyo, Japan.

[1] S. E. Woosley and R. E. Taam, Nature (London) **263**, 101 (1976).
[2] J. Grindlay, Comments Mod. Phys. C **6**, 165 (1976).
[3] D. Lamb and F. Lamb, Astrophys. J. **220**, 291 (1978).
[4] H. Schatz and K. Rehm, Nucl. Phys. **A777**, 601 (2006).
[5] A. Parikh, J. José, G. Sala, and C. Iliadis, Prog. Part. Nucl. Phys. **69**, 225 (2013).
[6] R. Cornelisse, J. Heise, E. Kuulkers, F. Verbunt, and J. in't Zand, Astron. Astrophys. **357**, L21 (2000).
[7] A. Cumming and L. Bildsten, Astrophys. J. Lett. **559**, L127 (2001).
[8] T. E. Strohmayer and E. F. Brown, Astrophys. J. **566**, 1045 (2002).
[9] A. Cumming and J. Macbeth, Astrophys. J. Lett. **603**, L37 (2004).
[10] L. Keek and A. Heger, Astrophys. J. **743**, 189 (2011).
[11] L. Keek, A. Heger, and J. J. M. in 't Zand, Astrophys. J. **752**, 150 (2012).
[12] E. F. Brown, L. Bildsten, and R. E. Rutledge, Astrophys. J. Lett. **504**, L95 (1998).
[13] R. E. Rutledge, L. Bildsten, E. F. Brown, G. G. Pavlov, and V. E. Zavlin, Astrophys. J. **514**, 945 (1999).
[14] E. M. Cackett, R. Wijnands, J. M. Miller, E. F. Brown, and N. Degenaar, Astrophys. J. Lett. **687**, L87 (2008).
[15] E. M. Cackett, E. F. Brown, A. Cumming, N. Degenaar, J. M. Miller, and R. Wijnands, Astrophys. J. Lett. **722**, L137 (2010).
[16] J. K. Fridriksson, J. Homan, R. Wijnands, M. Méndez, D. Altamirano, E. M. Cackett, E. F. Brown, T. M. Belloni, N. Degenaar, and W. H. G. Lewin, Astrophys. J. **714**, 270 (2010).
[17] D. Page and S. Reddy, Phys. Rev. Lett. **111**, 241102 (2013).
[18] N. Degenaar, Z. Medin, A. Cumming, R. Wijnands, M. T. Wolff, E. M. Cackett, J. M. Miller, P. G. Jonker, J. Homan, and E. F. Brown, Astrophys. J. **791**, 47 (2014).
[19] A. Turlione, D. N. Aguilera, and J. A. Pons, Astron. Astrophys. **577**, A5 (2015).
[20] L. Bildsten, Astrophys. J. Lett. **501**, L89 (1998).
[21] G. Ushomirsky, C. Cutler, and L. Bildsten, Mon. Not. R. Astron. Soc. **319**, 902 (2000).
[22] H. Schatz, L. Bildsten, A. Cumming, and M. Wiescher, Astrophys. J. **524**, 1014 (1999).
[23] J. Stevens, E. F. Brown, A. Cumming, R. H. Cyburt, and H. Schatz, Astrophys. J. **791**, 106 (2014).
[24] K. Sato, Prog. Theor. Phys. **62**, 957 (1979).
[25] O. Blaes, R. Blandford, and P. Madau, Astrophys. J. **363**, 612 (1990).
[26] P. Haensel and J. Zdunik, Astron. Astrophys. **227**, 431 (1990).
[27] S. Gupta, E. F. Brown, H. Schatz, P. Möller, and K.-L. Kratz, Astrophys. J. **662**, 1188 (2007).
[28] A. W. Steiner, Phys. Rev. C **85**, 055804 (2012).
[29] H. Schatz *et al.*, Nature (London) **505**, 62 (2014).
[30] G. Gamow and M. Schoenberg, Phys. Rev. **59**, 539 (1941).
[31] J. Homan, J. K. Fridriksson, R. Wijnands, E. M. Cackett, N. Degenaar, M. Linares, D. Lin, and R. A. Remillard, Astrophys. J. **795**, 131 (2014).
[32] A. T. Deibel, A. Cumming, E. F. Brown, and D. Page, Astrophys. J. **809**, L31 (2015).
[33] R. K. Wallace and S. E. Woosley, Astrophys. J. Suppl. Ser. **45**, 389 (1981).
[34] H. Schatz, A. Aprahamian, V. Barnard, L. Bildsten, A. Cumming, M. Ouellette, T. Rauscher, F.-K. Thielemann, and M. Wiescher, Phys. Rev. Lett. **86**, 3471 (2001).
[35] H. Schatz, L. Bildsten, and A. Cumming, Astrophys. J. Lett. **583**, L87 (2003).
[36] C. Langer *et al.*, Phys. Rev. Lett. **113**, 032502 (2014).
[37] G. Audi, M. Wang, A. Wapstra, F. Kondev, M. MacCormick, X. Xu, and B. Pfeiffer, Chin. Phys. C **36**, 1287 (2012).
[38] P. Moller, J. Nix, W. Myers, and W. Swiatecki, At. Data Nucl. Data Tables **59**, 185 (1995).
[39] M. Honma, T. Otsuka, B. Brown, and T. Mizusaki, Eur. Phys. J. A **25**, 499 (2005).
[40] S. Goriely, N. Chamel, and J. M. Pearson, Phys. Rev. C **82**, 035804 (2010).
[41] M. Matoš *et al.*, Nucl. Instrum. Methods Phys. Res., Sect. A **696**, 171 (2012).
[42] A. Estradé *et al.*, Phys. Rev. Lett. **107**, 172503 (2011).
[43] Z. Meisel and S. George, Int. J. Mass Spectrom. **349–350**, 145 (2013).
[44] Z. Meisel *et al.*, Phys. Rev. Lett. **114**, 022501 (2015).
[45] D. J. Morrissey, B. M. Sherrill, M. Steiner, A. Stolz, and I. Wiedenhoever, Nucl. Instrum. Methods Phys. Res., Sect. B **204**, 90 (2003).
[46] D. Bazin, J. Caggiano, B. Sherrill, J. Yurkon, and A. Zeller, Nucl. Instrum. Methods Phys. Res., Sect. B **204**, 629 (2003).
[47] D. Shapira, T. Lewis, and L. Hulett, Nucl. Instrum. Methods Phys. Res., Sect. A **454**, 409 (2000).
[48] F. Wienholtz *et al.*, Nature (London) **498**, 346 (2013).
[49] G. Audi, F. Kondev, M. Wang, B. Pfeiffer, X. Sun, J. Blachot, and M. MacCormick, Chin. Phys. C **36**, 1157 (2012).
[50] X. Tu, X. G. Zhou, D. J. Vieira, J. M. Wouters, Z. Y. Zhou, H. L. Seifert, and V. G. Lind, Z. Phys. A **337**, 361 (1990).
[51] M. Matoš, Ph.D. thesis, University of Giessen, 2004.
[52] A. Wapstra, G. Audi, and C. Thibault, Nucl. Phys. **A729**, 129 (2003).
[53] H. L. Crawford *et al.*, Phys. Rev. C **82**, 014311 (2010).
[54] S. N. Liddick *et al.*, Phys. Rev. C **70**, 064303 (2004).
[55] M. Kortelainen, T. Lesinski, J. Moré, W. Nazarewicz, J. Sarich, N. Schunck, M. V. Stoitsov, and S. Wild, Phys. Rev. C **82**, 024313 (2010).
[56] M. Kortelainen, J. McDonnell, W. Nazarewicz, P.-G. Reinhard, J. Sarich, N. Schunck, M. V. Stoitsov, and S. M. Wild, Phys. Rev. C **85**, 024304 (2012).
[57] A. L. Cole, T. S. Anderson, R. G. T. Zegers, S. M. Austin, B. A. Brown, L. Valdez, S. Gupta, G. W. Hitt, and O. Fawwaz, Phys. Rev. C **86**, 015809 (2012).